Analysis of the electric field gradient in the perovskites $SrTiO_3$ and $BaTiO_3$: Density functional and model calculations

K. Koch,[1] R. O. Kuzian,[2] K. Koepernik,[3] I. V. Kondakova,[2] and H. Rosner[4]
[1]*Max-Planck-Institut für Chemische Physik fester Stoffe, 01187 Dresden, Germany*
[2]*Institute for Problems of Materials Science, Krzhizhanovskogo 3, 03180 Kiev, Ukraine*
[3]*Leibniz Institute for Solid State and Materials Research, 01171 Dresden, Germany*
[4]*Max-Planck-Institute for Chemical Physics of Solids, 01187 Dresden, Germany*
(Received 18 May 2009; revised manuscript received 28 July 2009; published 16 September 2009)

We analyze recent measurements [R. Blinc, V. V. Laguta, B. Zalar, M. Itoh, and H. Krakauer, J. Phys.: Condens. Matter **20**, 085204 (2008)] of the electric field gradient on the oxygen site in the perovskites $SrTiO_3$ and $BaTiO_3$, which revealed, in agreement with calculations, a large difference in the electric field gradient (EFG) for these two compounds. In order to analyze the origin of this difference, we have performed density functional electronic-structure calculations within the local-orbital scheme FPLO. Our analysis reveals the counter-intuitive behavior that the EFG increases upon lattice expansion. Application of the standard model for perovskites, the effective two-level *p-d* Hamiltonian, cannot explain the experimentally observed and theoretically predicted behavior. In order to describe the EFG dependence correctly, a model beyond the usually sufficient *p-d* Hamiltonian is needed. We demonstrate that the counter-intuitive increase in the EFG upon lattice expansion can be explained by an *s-p-d* model containing the contribution of the oxygen 2*s* states to the crystal field on the Ti site. The proposed model extension is of general relevance for all related transition-metal oxides with similar crystal structure.

DOI: 10.1103/PhysRevB.80.125113 PACS number(s): 77.84.Dy, 76.60.−k, 77.80.−e

I. INTRODUCTION

Perovskitelike compounds ABO_3, with A being an alkali, alkaline-earth, or rare-earth metal and B a transition-metal element, attract much attention because of their importance for both fundamental science and technological applications.[1] Although the high-temperature cubic phase has a very simple crystal structure, this does not prevent these compounds from exhibiting a large variety of physical properties rendering the perovskites to model compounds for studies of a large variety of different physical phenomena. Within the perovskite family, we find superconductivity, e.g., in $K_xBa_{1-x}BiO_3$,[2] giant magnetoresistance, e.g., in $LaMnO_3$,[3] orbital ordering, e.g., in $YTiO_3$,[4] and ferroelectricity, e.g., in $BaTiO_3$.[1,5] The latter phenomenon is of large interest because of technological applications.

The compounds $SrTiO_3$ (STO) and $BaTiO_3$ (BTO) are isovalent. The valence and conduction bands of the two perovskites are formed by p states of oxygen and d states of titanium. In the high-temperature cubic phase (space group $Pm3m$), the Ti and O sublattices have the identical geometry for STO and BTO, the lattice parameters being $a=3.8996$ Å (Ref. 6) and $a=4.009$ Å,[1] respectively. As the temperature decreases, both compounds experience a softening of an optical-phonon mode, which corresponds to Ti motion toward the oxygen.[1] BTO exhibits a succession of phase transitions, from the high-temperature cubic perovskite phase to ferroelectric structures with tetragonal, orthorhombic, and rhombohedral symmetry.[1] In contrast, STO behaves as an incipient ferroelectric in the sense that it remains paraelectric down to the lowest temperatures, exhibiting nevertheless a very large static dielectric response. It undergoes an antiferrodistortive phase transition at 105 K to a tetragonal (space group $I4/mcm$) phase but this transition is of nonpolar character and has little influence on the dielectric properties.[7]

An appropriate tool to study even subtle structural changes is the electric field gradient (EFG) due to its high sensitivity with respect to changes in the local charge distribution. The EFG can be measured experimentally and calculated form first principles with high reliability and accuracy. A straightforward comparison of the measured and the calculated EFG values is possible without complex models in between, thus allowing a detailed, microscopically based analysis of the changes in the charge density, the underlying orbital occupation and the related implications for the picture of the chemical bonding.

The first experimental and theoretical determination of the ^{17}O electric field gradient on the oxygen site in perovskites was recently reported for STO and BTO, where the linearized augmented plane-wave (LAPW) method was used for the first-principle calculations. The most striking feature in the experimental and theoretical data is the large difference of the EFGs between the two compounds. The calculational investigation of Blinc *et al.*[8] concluded, that the magnitude of the EFG of ^{17}O in BTO is larger than the EFG of ^{17}O in STO due to two effects: (i) larger lattice parameters in BTO compared to STO and (ii) a larger ionic radius of Ba compared to Sr.

While the experimental determination (NMR) cannot provide the sign of the EFG, the LAPW calculation yielded a negative EFG. A negative EFG corresponds to a prolate electron density which implies the importance of covalence effects. In order to elucidate the origin of the sign of the EFG and the different contributions to the EFG, we have performed first-principle calculations using the density functional theory (DFT) based code full-potential local-orbital (FPLO).[9] Since the representation of the potential and the density in FPLO allows easy decomposition, FPLO is especially

TABLE I. The experimental and calculated values of the EFG (in 10^{21} V/m^2) on the oxygen site (^{17}O) in the cubic phase of the two perovskites. The last four lines refer to equations given in the Appendix.

	$SrTiO_3$	$BaTiO_3$	Ref.
$\lvert V_{zz}^{exp}\rvert$	1.62	2.46	Ref. 8
V_{zz}^{cal}	−1.00	−2.35	Ref. 8
V_{zz}^{cal}	1.00	2.44	Eq. (A10)
V_{zz}^{on}	−0.21	1.39	Eq. (A11)
V_{zz}^{off}	1.21	1.05	Eq. (A12)
$V_{zz,pp}^{on,net}$	96%	107%	Eq. (A15)

suited to address these questions. The calculational details of our investigation are given in Sec. II and the obtained results are presented in Sec. III. These results cannot be explained by intuitive models, which are also described in this section. Therefore, a more complex microscopic model Hamiltonian is introduced in Sec. IV. Using the properties of this extended *s*-*p*-*d*-type model, a consistent interpretation of the experimental data and the theoretical DFT results is provided and a deeper, microscopically based understanding is obtained.

II. CALCULATION METHODS

The electronic band-structure calculations were performed with the full-potential local-orbital minimum basis code FPLO (version 5.00–19) (Ref. 9) within the local-density approximation (LDA). In the scalar relativistic calculations the exchange and correlation potential of Perdew and Wang[10] was employed. As basis sets Ba ($4d5s5p/6s6p5d+4f7s7p$), Sr ($4s4p/5s5p4d+6s6p$), Ti ($3s3p3d/4s4p4d+5s5p$), and O ($2s2p3d+3s3p$) were chosen for semicore/valence +polarization states. The high-lying states improve the completeness of the basis which is especially important for accurate EFG calculations. The lower-lying states were treated fully relativistically and as core states. A well-converged k mesh of 455 k points was used in the irreducible part of the Brillouin zone.

III. BAND-STRUCTURE RESULTS

In FPLO, the EFG on a nucleus at a given lattice site may be represented as the sum of two contributions: An on-site contribution V_{zz}^{on} [see Eq. (A11)], which comes from the on-site contribution of the electron density of the given lattice site, and the off-site contribution V_{zz}^{off} [see Eq. (A12)], which results from the potential of all other atoms (see Appendix, Sec. 1). The on-site contribution V_{zz}^{on} can be split up into *p*-*p*, *s*-*d*, and *d*-*d* contributions (see Appendix, Sec. 2).

The on- and off-site contributions as well as their sum and the dominating *p*-*p* contribution [see Eq. (A15)] are shown in Table. I. Whereas the total EFG for ^{17}O in BTO agrees well with the experiment (1% deviation), the total EFG for ^{17}O in STO is in discrepancy[11] with the experiment (38% deviation), see Table. I. Compared to the EFGs calculated with the LAPW code in Ref. 8, we obtain almost the same

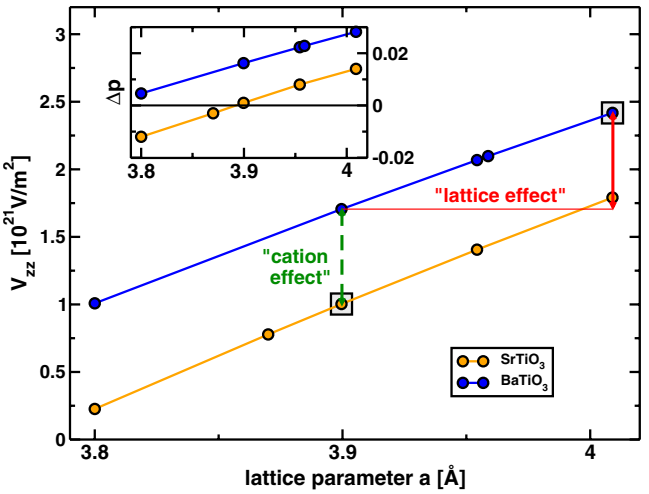

FIG. 1. (Color online) Calculated V_{zz} as a function of the lattice parameter a. V_{zz} for the experimental lattice parameter is marked by shaded squares. The "cation" and "lattice effect," which are responsible for the difference in V_{zz} for these two compounds are indicated by the dashed (green) and full (red) arrow, respectively. Inset: the anisotropy count Δp in dependence of the lattice parameter a in Å.

absolute value of V_{zz} but the opposite sign, see Table. I. Our calculated EFGs as a function of the lattice parameter a for both compounds reveal the same tendency as observed in Ref. 8: the absolute value of the EFG increases under the lattice expansion (see Fig. 1). From Fig. 1 we also conclude that the EFG of BTO is not only larger than the EFG of STO due to larger lattice parameters ("lattice effect"), but also due to an "cation effect," which is responsible for the remaining difference. This lattice effect is demonstrated by the shift between the two EFG curves in Fig. 1.

The increase in the (absolute value of the) EFG upon lattice expansion is rather counter intuitive. In the traditional approach, the spherically symmetric electronic shell of an ion is perturbed by the potential of the external (point) charges of the solid. As a result, the total EFG on the ion nucleus is caused by the EFG of the external potential and is roughly proportional to it. It is clear that this approach predicts the opposite tendency: the strength of the external potential is inversely proportional to the lattice constant and thus the (absolute value of the) EFG should decrease under the lattice expansion. The failure of this approach to describe the observed behavior of the EFG indicates that a fully ionic description of the perovskites is inappropriate.

In an alternative approach, the electronic shell of the atom is disturbed by the hybridization of the wave functions with the states of the surrounding atoms. The hybridization results in the asymmetry of the electronic cloud of the atom and the EFG on its nucleus. Apparently, this covalent approach predicts the same tendency as the ionic one: it is usually believed that the hybridization decreases with the increase in the bond length. In both approaches we may say: when expanding the lattice, we decrease its influence on the atom and the electronic shell should become closer to that of the free atom. Hence, we come to the conclusion: the (absolute value of the) EFG should decrease under the lattice expansion, which is opposite to the experimental observation and the

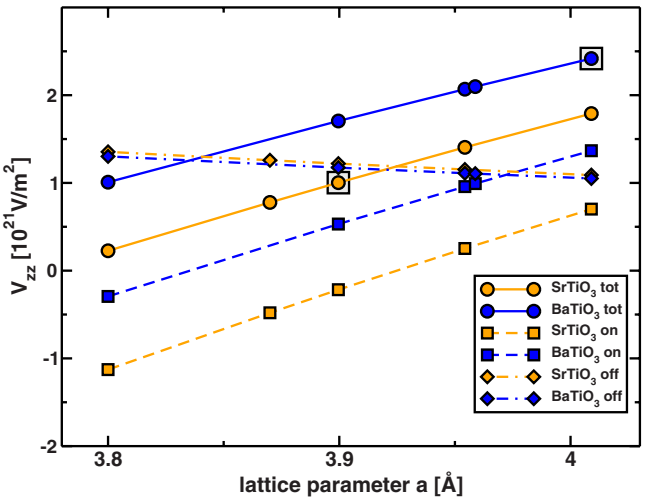

FIG. 2. (Color online) The on-site V_{zz}^{on}, off-site V_{zz}^{off}, and total EFG as a function of the lattice parameter a. The gray shaded squares mark the experimental lattice parameter.

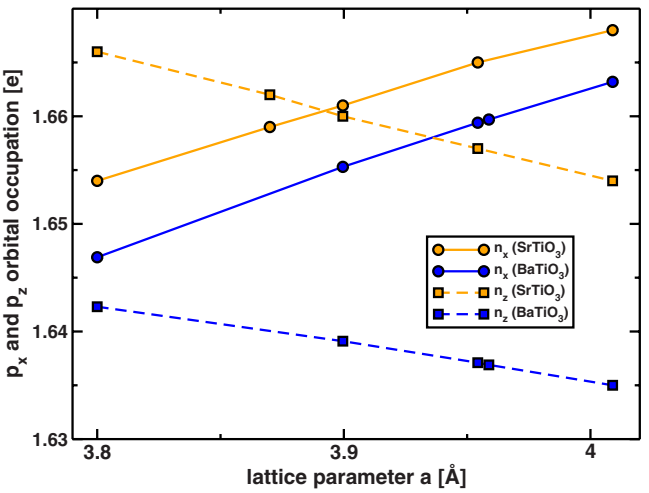

FIG. 3. (Color online) Occupation of p_x and p_z states in dependence of the lattice parameter a.

results of both first-principles calculations. We will tackle this problem in detail in Sec. IV.

Another problem is the different sign of the EFG obtained from the two different band-structure codes. If the sign of the EFG is taken into account, the slope in our graph (Fig. 1) is opposite to the slope in the graph obtained with the LAPW code (Fig. 5 in Ref. 8). Since the NMR experiment is not sensitive to the sign of the EFG, we will investigate the influence of the lattice expansion on the different contributions to the EFG to get more insight regarding this issue.

Our calculations show that both the on-site and the off-site contribution to the EFG have comparable values for the perovskite lattice, see Table. I and Fig. 2. In Fig. 2, the two contributions, V_{zz}^{on} (dashed line) and V_{zz}^{off} (dash-point line) and the total EFG (full line) are shown. Whereas the off-site EFG decreases only slightly upon lattice expansion, the on-site EFG increases strongly with increasing lattice parameters, resulting in the significant increase in the total EFG. We also observe that the off-site EFG is almost identical for these two structures, which is in line with the observed weak dependence of V_{zz}^{off} on the lattice parameters.

The on-site EFG is mainly caused by electrons with p character, see Table I. Therefore, we will investigate the corresponding anisotropy count Δp.[12] In the perovskite structure ABO_3, the oxygen site has axial symmetry, and the z axis is directed along the B-O bond. Thus, the anisotropy count is the difference between the population of the oxygen $2p$ σ (corresponds to p_z) and π (corresponds to $p_{x,y}$) orbitals. In the inset of Fig. 1, we see that the anisotropy count Δp increases with the lattice expansion. This is in agreement with the increasing on-site EFG. If we focus on BTO, where the experimental and calculated (for the experimental lattice parameter a=4.009 Å) values for the EFG agree very well, we see that this positive V_{zz} corresponds to a positive Δp. That means the p electron density (responsible for the EFG) has an oblate shape, since more electrons are occupying the $p_{x,y}$ orbitals than the p_z orbital, which is in agreement with the positive sign of the EFG.

After concluding that the sign of V_{zz} for ^{17}O for both STO and BTO should be positive, we come back to the counter-intuitive behavior of the increasing EFG upon lattice expansion. Figure 3 reveals that the increase in Δp with lattice expansion, which is responsible for the increasing EFG upon lattice expansion, is due to an increasing occupation of π (corresponds to $p_{x,y}$) and an decreasing population of σ (corresponds to p_z) orbitals.

IV. DISCUSSION

In order to understand this anomalous behavior of the σ orbital, we will analyze the main features of the electronic structure of perovskites. Detailed band-structure studies of perovskite compounds were performed by Mattheiss,[13–15] who also proposed a first tight-binding fit for the band dispersions. Wolfram *et al.*[16–18] (cf. also Ref. 19) developed a very simple model (Wolfram and Ellialtioglu, WE) for the valence and conduction bands, which reflects their basic properties. The WE model includes the d orbitals of the B ion and the p orbitals of the oxygen. Wolfram *et al.*[16–18] pointed out a quasi-two-dimensional character of the bands, which is due to the symmetry of the orbitals. If one retains only nearest-neighbor hoppings, the total 14×14 Hamiltonian matrix (five d orbitals and nine p orbitals) acquires block-diagonal form at each value of $\vec{k}$. The three 3×3 matrices describe the π_{ij} bands (ij=xy,yz,xz). Every d_{ij} orbital of the t_{2g} symmetry couples with its own combination of oxygen $2p$ π orbitals, which lie in the same plane perpendicular to the bond direction. They form a pair of bonding and antibonding states. The remaining combination of the $2p$ π orbitals in the same plane forms the nonbonding band. Wolfram *et al.* call this group of bands π bands. The states described by the 5×5 block matrix are called σ bands since they are formed by oxygen $2p$ σ orbitals, which are coupled with the e_g ($d_{x^2-y^2}$ and d_{z^2}) orbitals of the B ion. This matrix decouples into one nonbonding band and two pairs of bonding and antibonding bands.

Figure 4 shows the calculated band structure for STO for two different lattice parameters a. The features mentioned above are clearly seen (cf. Fig. 2 of Ref. 18). The antibond-

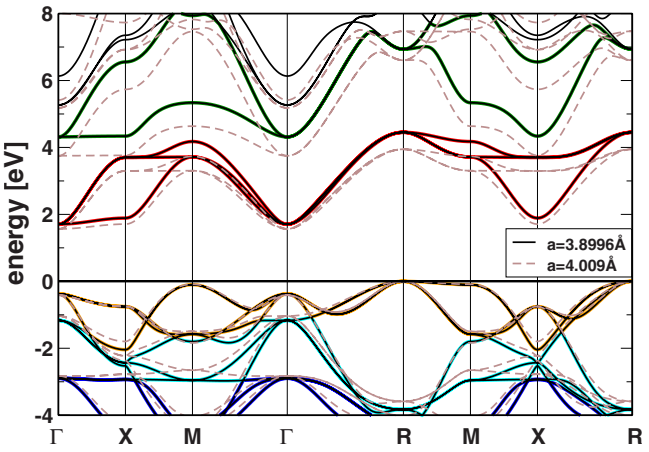

FIG. 4. (Color online) $SrTiO_3$: band structure for two different lattice parameters $a=3.8996$ Å (full lines) and $a=4.009$ Å (dashed lines). The different band characters are given by different colors: blue (bonding, σ), cyan (bonding, π), orange (nonbonding), red (antibonding, π_{ij}), and green (antibonding, d_{eg}), see text. Since it is not easy to interpret the valence band, the colors in the valence band are only approximate.

ing π_{ij} bands are situated between 2 and 4 eV, where the π_{yz} band is almost dispersionless in the direction $\Gamma \rightarrow X$. This manifests the quasi-two-dimensional character of the bands. The bands originating from the d e_g orbitals are in the range from 4 to 8 eV, where the band expressing d_{z^2} character is dispersionless along the $\Gamma \rightarrow X$ direction. The valence band has a more complex character due to additional mixing from the direct p-p hopping. This is neglected in the simple version of the WE model. Nevertheless, we see that the nonbonding bands lie on top of the valence band and have a much smaller dispersion than the bonding bands, which lie below −1 eV (π_{ij}) and below −3 eV (σ bands). The latter have a larger dispersion due to much larger d-p hoppings.

Although the Kohn-Sham theory is not good for excitation spectra, or obtaining the correct energy gap, it yields reliable occupation numbers, on-site energies and transfer integrals, especially in the absence of strong correlations. Therefore, we can use our LDA band structure to obtain reliable parameters as input for further treatment using model Hamiltonians.

In the following, we explore within the WE model how the occupation numbers and the resulting anisotropy count for the p orbitals depend on the lattice parameters. In dielectric compounds such as STO and BTO, the bonding and nonbonding states are fully occupied. Contrary to the nonbonding bands, which have almost pure p character, the bonding and antibonding bands are mixed p-d bands. The population of the p orbitals is given by the sum of the occupation numbers of the nonbonding and the bonding bands, whereof the latter are lattice-parameter dependent.

Every pair of bonding and antibonding states is described by an effective two-level model[17]

$$\hat{H}_m = \Delta_m(|d,\mathbf{k}\rangle\langle d,\mathbf{k}| - |p,\mathbf{k}\rangle\langle p,\mathbf{k}|) + V_m f_{m\mathbf{k}}(|d,\mathbf{k}\rangle\langle p,\mathbf{k}| + |p,\mathbf{k}\rangle\langle d,\mathbf{k}|). \quad (1)$$

Here, m describes the character of the band $m=\pi$ and σ, and $f_{m\mathbf{k}}$ is a dimensionless function, which depends on the dimensionless variable $\mathbf{k}a$ (note that $\mathbf{k}$ is measured in units of π/a, so neither $\mathbf{k}a$ nor $f_{m\mathbf{k}}$ depends on a). The state mixing is defined by the interplay of the on-site energy difference Δ_m and the transfer integral V_m, which determines the bandwidth of the corresponding band. The eigenstates of Hamiltonian (1) have the form

$$|\mathbf{k},\nu\rangle = c_{d\mathbf{k}\nu}|d,\mathbf{k}\rangle + c_{p\mathbf{k}\nu}|p,\mathbf{k}\rangle, \quad (2)$$

and the following energies and occupation numbers are obtained

$$E_{\mathbf{k}m\nu} = \nu\sqrt{\Delta_m^2 + V_m^2(f_{m\mathbf{k}})^2}, \quad \nu = \pm 1 \quad (3)$$

$$n_{p\mathbf{k}m\nu} \equiv 2|c_{p\mathbf{k}\nu}|^2 = 1 - \Delta_m/E_{\mathbf{k}\nu}. \quad (4)$$

$$n_{d\mathbf{k}m\nu} \equiv 2|c_{d\mathbf{k}\nu}|^2 = 2(1-|c_{p\mathbf{k}\nu}|^2) = 1 + \frac{\Delta_m}{E_{\mathbf{k}\nu}}. \quad (5)$$

Here, $\nu=+1$ describes the antibonding and $\nu=-1$ describes the bonding band. In this two-level system, two asymptotic behaviors are possible. First, $\Delta_m/V_m \rightarrow \infty$, which yields for the occupation numbers of the bonding bands $n_{p\mathbf{k}m,-1} \rightarrow 2$ and $n_{d\mathbf{k}m,-1} \rightarrow 0$. In this case, both electrons are in the p state of the ligand ion and d states are empty, called the ionic limit. Second, $\Delta_m/V_m \rightarrow 0$, which yields for the occupation numbers $n_{p\mathbf{k}m,-1} \rightarrow 1$ and $n_{d\mathbf{k}m,-1} \rightarrow 1$. In this case, the electrons are equally shared by the p, and d states. This is the covalent limit. From the trends in Fig. 3, we observe that while the population of the p_π orbitals increases, the population of the p_σ orbitals decreases. This means the Ti-O π bond gets more ionic with lattice expansion (as expected) whereas the Ti-O σ bond gets more covalent, which we will try to explain with this model.

The parameters of this model can be extracted from the band energies at symmetry points of the Brillouin zone in Fig. 4 (see Appendix, Sec. 3 for more details). For example, the on-site energy differences Δ_m can be obtained from the Γ point, since due to symmetry, the d-p mixing vanishes at this point and the band states acquire a pure d or p character. For $a=3.8996$ Å we have for STO $E_{d_{t2g}} \approx 1.7$ eV, $E_{d_{eg}} \approx 4.3$ eV, and $E_p \approx -1.2$ eV. This yields [using Eqs. (A25) and (A26)] $2\Delta_\pi = E_{d_{t2g}} - E_p \approx 2.9$ eV and $2\Delta_\sigma = E_{d_{eg}} - E_p \approx 5.5$ eV. From these values and the f_{mk} as given in Refs. 17 and 18 we obtain the Slater-Koster hopping parameters $V_\sigma \approx 2.1$ eV Eq. (A28), $V_\pi = V_{pd\pi} \approx 1.6$ eV Eq. (A27), and $V_{pd\sigma} \approx 2.7$ eV Eq. (A30).[20]

Since the occupation numbers of the nonbonding bands do not depend on the lattice parameter and the antibonding bands ($\nu=+1$) are not occupied, we consider the bonding bands ($\nu=-1$) only. The contributions from the bonding bands to the population of the p_m orbitals n_{p_m} are obtained by a sum over the Brillouin zone. In order to analyze the occupation as a function of the lattice expansion, we need the derivative of the occupation number with respect to the lattice parameter a. From Eq. (4) we obtain for the derivative (denoted by $'$)

$$n'_{p\mathbf{k}m,-1} = \frac{V_m^2 (f_{m\mathbf{k}})^2 \Delta_m}{[\sqrt{\Delta_m^2 + V_m^2 (f_{m\mathbf{k}})^2}]^3} \left(\frac{\Delta'_m}{\Delta_m} - \frac{V'_m}{V_m} \right). \quad (6)$$

The derivative of n_{p_m} is proportional to

$$n'_{p_m} \propto \left(\frac{\Delta'_m}{\Delta_m} - \frac{V'_m}{V_m} \right). \quad (7)$$

Figure 3 shows that n'_{p_m} has a different behavior for $m=\sigma$ (n'_{p_σ} is negative) and $m=\pi$ (n'_{p_π} is positive). Thus, within the WE model, the observed increase in the EFG, which is due to the decreasing occupation of the p_σ orbitals would yield

$$-\frac{V'_\sigma}{V_\sigma} < -\frac{\Delta'_\sigma}{\Delta_\sigma}. \quad (8)$$

Both Δ_σ and V_σ decrease upon lattice expansion: Fig. 4 shows that the energies at the Γ point $E_{d_{eg}}$ and $E_{d_{t2g}}$ and the bandwidths are smaller for the larger lattice parameter a =4.009 Å, than for the smaller lattice parameter a =3.8996 Å. A commonly accepted estimate[21] for the dependence of hopping integrals on a is $V_\sigma \propto a^{-\alpha}$ with α between 3.5 and 4 (from the LDA band structure, we obtain α $=3.5 \pm 0.5$). This gives

$$-a\frac{V'_\sigma}{V_\sigma} = \alpha \geq 3. \quad (9)$$

Δ_σ is the difference in energy of the atomic levels corrected by the crystal field (CF) (Ref. 22) $\Delta_\sigma = \varepsilon_d - \varepsilon_p + \delta_{\mathrm{CF},\sigma}$. The crystal field consists of two contributions:[23] A (dominating) electrostatic contribution, which is the difference of the Madelung potentials of Ti and O, hence $\delta_{\mathrm{CF},el} \propto a^{-1}$ and a hybridization contribution, which, in our case (octahedral coordination), contains a large and strongly a-dependent contribution for $m=\sigma$ from the semicore s states of the ligand. Indeed, (cf. Fig. 4) the change due to the increasing lattice parameter a is much larger for Δ_σ than for Δ_π. The main electrostatic contribution, which implies $\delta_{\mathrm{CF},el} \propto a^{-1}$, leads to

$$-a\frac{\Delta'_\sigma}{\Delta_\sigma} = \frac{\delta_{\mathrm{CF},el}}{\Delta_\sigma}.$$

Since $\varepsilon_d - \varepsilon_p + \delta_{\mathrm{CF},el} > \delta_{\mathrm{CF},el}$ is $\delta_{\mathrm{CF},el}/\Delta_\sigma < 1$ and therefore

$$-a\frac{\Delta'_\sigma}{\Delta_\sigma} < 1. \quad (10)$$

Combining the estimates from Eqs. (9) and (10), we get

$$-a\frac{\Delta'_\sigma}{\Delta_\sigma} < 1 < 3 \leq -a\frac{V'_\sigma}{V_\sigma}. \quad (11)$$

This is in contradiction to the inequality Eq. (8), leading to the conclusion that the WE model, though consistent with the intuitive expectations (see Sec. III) is unable to predict the observed behavior of the σ-orbital occupation in Fig. 3.

A possible reason for the failure of the WE model is that according to Ref. 15, a large contribution to the CF comes from the oxygen 2s orbitals, which lie almost 18 eV below the Ti 3d level, Δ_{sd}=17.9 eV, but have a large matrix element $V_{sd\sigma}$=3.0 eV with the e_g orbitals. This suggests to extend the WE model taking into account the oxygen 2s states in order to explain the increasing EFG upon lattice expansion. This is Harrison's model, where $V_{sd\sigma}$ is obtained from Eq. (A29)

$$\Gamma_{12} = \frac{\varepsilon_s + \varepsilon_d}{2} \pm \sqrt{\left(\frac{\varepsilon_s - \varepsilon_d}{2} \right)^2 + 6V_{sd\sigma}^2},$$

with ε_s=−16.2 eV, ε_d=1.7 eV, and Γ_{12}=4.3 taken from the band structure.

Taking the s orbitals into account, V_σ in the inequality Eq. (8) is replaced by $V_{sd\sigma}$. Harrison[21] argues that the a dependence of $V_{sd\sigma}$ is similar to the a dependence of $V_{pd\sigma}$. This suggestion is confirmed by our LDA calculations. Thus, we obtain

$$\frac{V'_{sd\sigma}}{V_{sd\sigma}} = -\frac{\alpha}{a}. \quad (12)$$

On the right-hand side we have the on-site energy difference, which is given by $\Delta_\sigma \approx \Delta_\pi + 3V_{sd\sigma}^2/\Delta_{sd}$, cf. Eq. (A33). The derivative of this expression is

$$\Delta'_\sigma \approx \frac{6}{\Delta_{sd}} V_{sd\sigma} V'_{sd\sigma}. \quad (13)$$

Note, that here we assumed $\Delta'_\pi = \Delta'_{sd} = 0$. Applying Eqs. (12) and (13) yields

$$-\frac{\Delta'_\sigma}{\Delta_\sigma} = \frac{\alpha}{a} \frac{6V_{sd\sigma}^2}{\Delta_{sd}\Delta_\pi + 3V_{sd\sigma}^2}. \quad (14)$$

Inserting Eqs. (12) and (14) in the inequality Eq. (8), we obtain within the Harrison model the observed increase in the EFG, due to the decreasing occupation of the p_σ orbitals, if the following inequality is fulfilled

$$\frac{\alpha}{a} = -\frac{V'_{sd\sigma}}{V_{sd\sigma}} \overset{!}{<} -\frac{\Delta'_\sigma}{\Delta_\sigma} = \frac{\alpha}{a} \frac{6V_{sd\sigma}^2}{\Delta_{sd}\Delta_\pi + 3V_{sd\sigma}^2} \Leftrightarrow \frac{1}{3}\Delta_{sd}\Delta_\pi \overset{!}{<} V_{sd\sigma}^2. \quad (15)$$

Using the values obtained from the LDA band structure ($V_{sd\sigma}$=3.0 eV, Δ_{sd}=17.9 eV, and Δ_π=1.4), we see that Eq. (15) is fulfilled. Thus, the inequality Eq. (8) holds for the STO σ orbitals and the observed negative slope of n_z in Fig. 3 can be understood.

After revealing the origin of the counter-intuitive behavior of the on-site EFG, we will discuss the unusually large value of the off-site EFG of the considered compounds. The dependence of this contribution with respect to the lattice parameter can be estimated in the following way: from the multipole expansion of a potential of a given ion, the sum of the monopole contributions to $v^{off}(\mathbf{r})$ Eq. (A6) has the slowest convergence. This contribution may be calculated within a point-charge model (PCM). Therefore, we note that the V_{zz} value created at the origin by a unit charge situated at the point $\mathbf{R}$ equals the value of the z component of the electric field E_z, created at the origin by the unit dipole directed along z axis and situated at the same point $\mathbf{R}$: $V_{zz} = (3Z^2 - R^2)/R^5$. That means, for the calculation of the EFG within the PCM, we need the electric field $S(\mathbf{r})$ of dipoles located at the sites $\mathbf{R}$, which are polarized along the z direction and

whose polarization is unity, at various points $\mathbf{r}$ through the cubic lattice: $S(\mathbf{r})=\Sigma_{\mathbf{R}}E_z(\mathbf{R}-\mathbf{r})$. Here, $\mathbf{r}=a(x,y,z)$ and $\mathbf{R}=a(l,m,n)$ with a being the lattice parameter and $l,m,n=0,\pm1,\pm2$. Using Eq. 16 of Ref. 24, we obtain for the EFG in the PCM at the oxygen site

$$V_{zz}^{\mathrm{PCM}}=-\frac{e}{a^3}\left[n_{\mathrm{Ti}}S\left(0,0,\frac{1}{2}\right)+n_AS\left(\frac{1}{2},\frac{1}{2},0\right)+2n_{\mathrm{O}}S\left(0,\frac{1}{2},\frac{1}{2}\right)\right]$$

$$=-\frac{e}{a^3}[30.080n_{\mathrm{Ti}}-8.668(n_A-n_{\mathrm{O}})]. \quad (16)$$

Here, n_{Ti} is the monopole moment of the ionicity of Ti. If we insert the charges of the Ti ion n_{Ti}, the O ion n_{O}, and the A ion $n_A=-(n_{\mathrm{Ti}}+3n_{\mathrm{O}})$ (with A=Sr and Ba) obtained from the FPLO calculations, we obtain, e.g., for STO $V_{zz}^{\mathrm{PCM}}=1.30\times10^{21}$ V/m^2. This value is very close to $V_{zz}^{off}=1.19\times10^{21}$ V/m^2, see Table. I. So, we obtain a good agreement for the EFGs obtained from the simple PCM model and the more complex calculation. This means, the FPLO code yields realistic relations of the charge distributions.

The prefactor e/a^3 in Eq. (16) is responsible for the observed decrease in the off-site contribution in case of lattice expansion, see Fig. 2. Also the charge redistribution may change the value of V_{zz}^{off}, but as we see in Fig. 2, it has a minor effect: the off-site EFG for BTO is smaller than for STO but the distance between the two curves is smaller than the lattice-parameter dependence of the two curves.

V. SUMMARY AND CONCLUSION

In summary, we have performed first-principle calculations of the electric field gradient on the oxygen site for $BaTiO_3$ and $SrTiO_3$ for different lattice parameters a. The values of our calculated EFGs agree well with the measured and, apart from the sign,[25] with the calculated (LAPW) counterparts from Ref. 8.

Decomposition of the EFG yields a large on-site contribution originating from the oxygen $2p$ shell. The on-site EFG reveals an anomalous dependence of the p_σ-orbital population on the lattice parameter a: the population decreases with lattice expansion, i.e., the p-d hybridization grows with increasing Ti-O distance. Simple ionic and covalent approaches lead to the conclusion that this behavior is counter intuitive. Also the effective two-level Hamiltonian proposed by Wolfram and Ellialtioglu, which describes the relevant states of the valence region (oxygen p and titanium d states) fails to describe the observed behavior of the EFG upon lattice expansion. Only the inclusion of the O $2s$ states to the crystal field results in a consistent picture: In fact, lattice expansion causes a charge transfer from the p_σ to the s orbitals of oxygen, whereas the population of the oxygen π orbitals increases with a. This charge redistribution leads to the increase in the EFG, which is the main reason for the surprisingly large difference of the EFGs between $BaTiO_3$ and $SrTiO_3$.

We expect that the observed feature, the increase in the anisotropy count of the p shell with the bond length, is common to all d-metal-oxygen bonds and should be taken into account accordingly in the interpretation of the relevant experiments. The considered $ATiO_3$ systems are not strongly correlated since the Ti $3d$ shell is formally empty. For magnetic ions with partially filled d shells, the influence of the O $2s$ orbitals will be diminished because the charge-transfer energy Δ_{sd} will include the on-site Coulomb repulsion within the d shell.

As a side effect, our investigation sounds a note of caution: when performing a mapping of a complex DFT bandstructure calculation onto a microscopically based minimal model in order to gain deeper physical understanding, care has to be taken that all relevant interactions are included.

ACKNOWLEDGMENTS

The authors thank the Heisenberg-Landau program, "DNIPRO" (Contracts No. 14182XB and No. M/98-2007), CNRS-NASU program PICS (Contract. No. 4767), and the SPP 1178 of the Deutsche Forschungsgemeinschaft for financial support. Discussions with V. V. Laguta and Alim Ormeci are gratefully acknowledged.

APPENDIX

1. EFG implementation in FPLO

The EFG is a local property. It is a traceless symmetric tensor of rank two, defined as the second partial derivative of the potential $v(\mathbf{r})$ evaluated at the position of the nucleus

$$V_{ij}\equiv\left(\frac{\partial^2v(\mathbf{r})}{\partial_i\partial_j}-\frac{1}{3}\delta_{ij}\Delta v(\mathbf{r})\right)\Bigg|_{\mathbf{r}=0}. \quad (A1)$$

With the definition

$$V_{2m}\equiv\sqrt{\frac{15}{4\pi}}\lim_{r\to0}\frac{1}{r^2}v_{2m}(r), \quad (A2)$$

can the Cartesian EFG tensor Eq. (A1) also be expressed in (real) spherical components $(l=2,m=\pm2,\pm1,0)$

$$V_{ij}=\begin{pmatrix} V_{22}-\frac{1}{\sqrt{3}}V_{20} & V_{2,-2} & V_{21} \\ V_{2,-2} & -V_{22}-\frac{1}{\sqrt{3}}V_{20} & V_{2,-1} \\ V_{21} & V_{2,-1} & \frac{2}{\sqrt{3}}V_{20} \end{pmatrix}. \quad (A3)$$

In FPLO, the EFG on a nucleus at a given lattice site $\mathbf{s}_0$ may be represented as the sum of two contributions

$$V_{ij}\equiv\left(\frac{\partial^2}{\partial_i\partial_j}-\frac{1}{3}\delta_{ij}\Delta\right)[v^{on}(\mathbf{r})+v^{off}(\mathbf{r})] \quad (A4)$$

$$v^{on}(\mathbf{r})=\sum_L\int d^3\mathbf{r}'\frac{n_{\mathbf{s}_0,L}(|\mathbf{r}'|)Y_L(\mathbf{r}')}{|\mathbf{r}-\mathbf{s}_0-\mathbf{r}'|}, \quad (A5)$$

$$v^{off}(\mathbf{r}) = \sum_{\mathbf{R}+\mathbf{s}\neq\mathbf{s}_0,L} \int d^3\mathbf{r}' \frac{n_{\mathbf{s},L}(|\mathbf{r}'|)Y_L(\mathbf{r}')}{|\mathbf{r}-\mathbf{R}-\mathbf{s}-\mathbf{r}'|} - \sum_{\mathbf{R}+\mathbf{s}\neq\mathbf{s}_0} \frac{Z_\mathbf{s}}{|\mathbf{r}-\mathbf{R}-\mathbf{s}|}, \tag{A6}$$

where Y_L are the (real) spherical harmonics; $\mathbf{R}$ is a Bravais vector, and $\mathbf{s}$ is an atom position in the unit cell. The index $L=nlm$ also absorbs the spin and the principal quantum number. The first term in Eq. (A4), the on-site contribution, comes from the on-site contribution of the electron density of the site $\mathbf{s}_0$, and the second term, the off-site contribution, comes from the potential of all other atoms.

Since the angular-momentum components of the local charge density give rise to multipole moments, which determine the Coulomb potential for large distances, FPLO uses the Ewald method to handle the long-range interactions (see Ref. 9, Sec. II D). The density is modified with a Gaussian auxiliary density $\tilde{n}_l(r)=n_l(r)-n_l^{\mathrm{Ew}}(r)$.[26] Inserting this modified density in the potentials Eqs. (A5) and (A6) yields

$$v(\mathbf{r}) = \tilde{v}^{on}(\mathbf{r}) + v^{\mathrm{Ew},on}(\mathbf{r}) + \tilde{v}^{off}(\mathbf{r}) + v^{\mathrm{Ew},off}(\mathbf{r}). \tag{A7}$$

These contributions are calculated to get the total EFG.

The first contribution is $\tilde{v}^{on}(\mathbf{r})$ in Eq. (A7). This potential is given by Eq. (A5) using the modified density $\tilde{n}_{\mathbf{s}_0,L}(r')$. The corresponding $\tilde{v}_{\mathbf{s}_0,2m}(r)$ components needed in Eq. (A2) are obtained from the solution of the radial Poisson equation [see Ref. 9 and Eq. (A33)]

$$\tilde{v}_{\mathbf{s}_0,L}(r) = \frac{4\pi}{2l+1}\left[\frac{1}{r^{l+1}}\int_0^r dx x^{l+2}\tilde{n}_{\mathbf{s}_0,L}(x) + r^l\int_r^\infty dx x^{-l+1}\tilde{n}_{\mathbf{s}_0,L}(x)\right].$$

Using l'Hôpital's rule, we obtain for the $\tilde{V}_{2m}^{on}$ component (from which $\tilde{V}_{ij}^{on}$ is obtained)

$$\tilde{V}_{2m}^{on} = 2\sqrt{\frac{3\pi}{5}}\left[\frac{n_{\mathbf{s}_0,2m}(0)}{5} + \int_0^\infty dx x^{-1}\tilde{n}_{\mathbf{s}_0,2m}(x)\right]. \tag{A8}$$

The first term in Eq. (A8) is the $2m$ component of the electronic density at the nucleus $n_{\mathbf{s}_0,2m}(0)\equiv\tilde{n}_{\mathbf{s}_0,2m}(0)$. The n_{2m} component of a spherical harmonic expansion of an analytic function around a given point behaves as $n_{2m}=\mathcal{O}(r^2)$. The only nonanalyticities of the electron density are caused by the spherical singularities of the nuclear potential and this cannot be aspherical. Therefore $n_{2m}(0)=0$, which can be shown explicitly both in a nonrelativistic and full relativistic theory.

The second contribution is $\tilde{v}^{off}(\mathbf{r})$ in Eq. (A7). This potential is given by Eq. (A6) using the modified density $\tilde{n}_{\mathbf{s},L}(r')$. Since the density $n_{\mathbf{s},2m}$ is not given at the site $\mathbf{s}_0$, where the atom under consideration is sitting, this equation has to be expanded. This can be done explicitly but the derivation as well as the result for $\tilde{V}_{ij}^{off}$ are very lengthy[27] and therefore not given here.

The remaining contributions are $v^{\mathrm{Ew},on}(\mathbf{r})+v^{\mathrm{Ew},off}(\mathbf{r})$ in Eq. (A7), which have to be calculated from the Ewald density alone. The auxiliary density $n_l^{\mathrm{Ew}}(\mathbf{r})$ is given as a Fourier expansion, resulting in the Ewald potential in Fourier space $v_\mathbf{G}^{\mathrm{Ew}}=\frac{4\pi}{|\mathbf{G}|^2}n_\mathbf{G}^{\mathrm{Ew}}$, Eq. (52) in Ref. 9. V_{ij}^{Ew} is obtained by differentiating $v^{\mathrm{Ew}}(\mathbf{r})=\Sigma_\mathbf{G}e^{i\mathbf{G}\mathbf{s}}v_\mathbf{G}^{\mathrm{Ew}}$

$$V_{ij}^{\mathrm{Ew}} = -\sum_\mathbf{G}\left(G_iG_j - \frac{1}{3}\mathbf{G}^2\delta_{ij}\right)\Re(e^{i\mathbf{G}\mathbf{s}}v_\mathbf{G}^{\mathrm{Ew}}). \tag{A9}$$

The total EFG tensor V_{ij} is given by the sum of these three contributions

$$V_{ij} = \tilde{V}_{ij}^{on} + \tilde{V}_{ij}^{off} + V_{ij}^{\mathrm{Ew}}. \tag{A10}$$

In order to analyze the on-site and off-site contributions, we define the on-site EFG as being the first term in Eq. (A4) but calculated from the unmodified density

$$V_{2m}^{on} = 2\sqrt{\frac{3\pi}{5}}\int_0^\infty dx x^{-1}n_{\mathbf{s}_0,2m}(x). \tag{A11}$$

The off-site EFG then is taken to be

$$V_{2m}^{off} = V_{2m} - V_{2m}^{on}. \tag{A12}$$

2. Orbital contributions to the EFG

In FPLO the electron density is separated into a net density and an overlap density (see Ref. 9, Sec. II B). The dominating net density is calculated from two orbitals at the same site $\mathbf{R}+\mathbf{s}=\mathbf{R}'+\mathbf{s}'=\mathbf{s}_0$

$$n_{\mathbf{s}_0}^{net}(\mathbf{r}) = \sum_{\mathbf{k},nL_1,L_2}^{occ} c_{\mathbf{s}_0L_1}^{\mathbf{k},n}\varphi_{\mathbf{s}_0,L_1}(\mathbf{r}-\mathbf{s}_0)\cdot c_{\mathbf{s}_0L_2}^{\star\mathbf{k},n}\varphi_{\mathbf{s}_0,L_2}(\mathbf{r}-\mathbf{s}_0).$$

The basis functions $\varphi_{\mathbf{s}_0,L}$ are localized on the lattice sites

$$\varphi_{\mathbf{s}_0,L}(\mathbf{r}-\mathbf{s}_0) \equiv \phi_{\mathbf{s}_0}^l(|\mathbf{r}-\mathbf{s}_0|)Y_L(\mathbf{r}-\mathbf{s}_0).$$

The $2m$ component of the radial net density needed for the contributions of the net EFG, can be calculated from

$$n_{\mathbf{s}_0,2m}^{net}(r) = \int n_{\mathbf{s}_0}^{net}(\mathbf{r})Y_{2m}(\mathbf{r}-\mathbf{s}_0)d\Omega = \sum_{L_1,L_2} c_{L_1L_2}\phi_{\mathbf{s}_0}^{l_1}(|\mathbf{r}-\mathbf{s}_0|)\phi_{\mathbf{s}_0}^{l_2}(|\mathbf{r}-\mathbf{s}_0|)G_{l_1,l_2,2}^{m_1,m_2,m}, \tag{A13}$$

where $G_{l_1,l_2,2}^{m_1,m_2,m}$ are the Gaunt coefficients and $c_{L_1L_2}=\Sigma_{\mathbf{k},n}c_{\mathbf{s}_0L_1}^{\mathbf{k},n}c_{\mathbf{s}_0L_2}^{\star\mathbf{k},n}$. Due to the properties of the Gaunt coefficients, $n_{\mathbf{s}_0,2m}^{net}$ consists only of p-p, d-d, and s-d (and if present p-f and f-f) contributions. These contributions to the on-site net EFG $V_{zz}^{on,net}$ are obtained by inserting Eq. (A13) into Eq. (A11). E.g., the p-p contribution $V_{2m,pp}^{on,net}$ is calculated from

$$V_{2m,pp}^{on,net} = 2\sqrt{\frac{3\pi}{5}}\int_0^\infty dx x^{-1}n_{\mathbf{s}_0,2m}^{net,pp}(x)$$

$$n_{\mathbf{s}_0,2m}^{net,pp}(x) = [\phi_{\mathbf{s}_0}^1(x)]^2\sum_{m_1,m_2} c_{1,1}^{m_1,m_2}G_{1,1,2}^{m_1,m_2,m}. \tag{A14}$$

The main component $V_{zz,pp}^{on,net}=\frac{2}{\sqrt{3}}V_{20,pp}^{on,net}$ is calculated from

TABLE II. The energies at the Γ and X points in $SrTiO_3$ given in eV. Here, $\Gamma_1 \approx \varepsilon_s$, $\Gamma_{25} \approx \varepsilon_p$, $\Gamma'_{25} = E_{d_{t2g}} \approx \varepsilon_d$, and $\Gamma_{12} = E_{d_{eg}}$.

a [Å]	Γ_{12}	Γ_1	Γ_{15}	Γ_{25}	Γ_{15}	Γ'_{25}	Γ_{12}	X_5	X_1
3.8996	−17.199	−16.177	−2.891	−1.166	−0.372	1.709	4.319	3.705	6.551
4.009	−16.923	−15.968	−2.828	−1.046	−0.408	1.579	3.800	3.332	5.798

$$n^{net,pp}_{\mathbf{s_0},20}(x) = \sqrt{\frac{1}{5\pi}}[\phi^1_{\mathbf{s}_0}(x)]^2 \sum_{\mathbf{k},n} \left[c^{\mathbf{k},n}_{\mathbf{s_0},1,0} c^{\star\mathbf{k},n}_{\mathbf{s_0},1,0} - \frac{1}{2}(c^{\mathbf{k},n}_{\mathbf{s_0},1,-1} c^{\star\mathbf{k},n}_{\mathbf{s_0},1,-1} + c^{\mathbf{k},n}_{\mathbf{s_0},1,1} c^{\star\mathbf{k},n}_{\mathbf{s_0},1,1}) \right]. \quad \text{(A15)}$$

We see, that this density is proportional to the difference of occupation in p_z ($m=0$) and $p_{x,y}$ ($m=\pm 1$) states, which is the anisotropy count.

3. Background for Sec. IV

In order to extract the parameters from the band structure we need the total Hamiltonian

$$\hat{H} = \sum_m [\hat{H}_m + e_m(|d,\mathbf{k}\rangle\langle d,\mathbf{k}| + |p,\mathbf{k}\rangle\langle p,\mathbf{k}|)]. \quad \text{(A16)}$$

Here, $\hat{H}_m$ is the Hamiltonian given in Eq. (1) and e_m is the mean energy of a pair of bands. The energies are therefore obtained from

$$E_{\mathbf{k}m\nu} + e_m = e_m + \nu\sqrt{\Delta_m^2 + V_m^2 (f_{m\mathbf{k}})^2}. \quad \text{(A17)}$$

For the three pairs of the π_{ij} bands, $f_{m\mathbf{k}}$ is given by

$$f^2_{\pi_{ij}\mathbf{k}} = 2(2 - C_i - C_j), \quad \text{(A18)}$$

with $C_i \equiv \cos(k_i a)$. The two σ bands are distinguished by the index $\lambda = \pm 1$ and $f_{m\mathbf{k}}$ is

$$f^2_{\sigma_\lambda \mathbf{k}} = 3 - C_x - C_y - C_z + \lambda(C_x^2 + C_y^2 + C_z^2 - C_x C_y - C_x C_z - C_y C_z)^{1/2}. \quad \text{(A19)}$$

Inserting these in Eq. (A17) for the Γ point ($\mathbf{k}a=0$) and the X point, ($k_x a = \pi, k_y = k_z = 0$), we obtain

$$\Gamma_{25} = e_\pi - \Delta_\pi = e_\sigma - \Delta_\sigma, \quad \text{(A20)}$$

and $\Gamma_{25} \equiv E_p \approx \varepsilon_p$

$$\Gamma'_{25} = e_\pi + \Delta_\pi, \quad \text{(A21)}$$

and $\Gamma'_{25} \equiv E_{d_{t2g}} \approx \varepsilon_d$

$$\Gamma_{12} = e_\sigma + \Delta_\sigma, \quad \text{(A22)}$$

and $\Gamma_{12} \equiv E_{d_{eg}}$

$$X_5 = e_\pi + \sqrt{\Delta_\pi^2 + 4V_\pi^2}, \quad \text{(A23)}$$

$$X_1 = e_\sigma + \sqrt{\Delta_\sigma^2 + 4V_\sigma^2}. \quad \text{(A24)}$$

Here, ε denotes the energy of the atomic level and E denotes the energy level corrected by a "crystal field" δ_{CF}, see below.

Now it is trivial to find the parameters Δ_m, V_m

$$2\Delta_\pi = \Gamma'_{25} - \Gamma_{25} \equiv E_{d_{t2g}} - E_p, \quad \text{(A25)}$$

$$2\Delta_\sigma = \Gamma_{12} - \Gamma_{25} \equiv E_{d_{eg}} - E_p = \varepsilon_d - \varepsilon_p + \delta_{\mathrm{CF}}, \quad \text{(A26)}$$

$$4V_\pi^2 = (X_5 - \Gamma'_{25})(X_5 - \Gamma_{25}), \quad \text{(A27)}$$

$$4V_\sigma^2 = (X_1 - \Gamma_{12})(X_1 - \Gamma_{25}). \quad \text{(A28)}$$

The energy values at the different Γ and X points for $SrTiO_3$ are given in Table. II.

So far, we have used the WE model, i.e., we have taken into account only the oxygen p and the titanium d states. Since this model is not sufficient to explain the observed behavior of the oxygen p_σ states, we have to expand the model. Harrison's model[21] includes also the oxygen s states. The s states change the dispersion in the σ bands, so that we have two parameters $V_{pd\sigma}$ and $V_{sd\sigma}$ instead of just one V_σ. Thus, the expressions become more complex, even at the symmetry points. In this model, the Eqs. (A20), (A21), and (A23) remain the same and the parameters ε_p, ε_d, and V_π are unchanged. For Γ_{12} Eq. (A22) and X_1 Eq. (A24), Harrison obtains

$$\Gamma_{12} = \frac{\varepsilon_d + \varepsilon_s}{2} + \sqrt{\left(\frac{\varepsilon_d - \varepsilon_s}{2}\right)^2 + 6V^2_{sd\sigma}}, \quad \text{(A29)}$$

$$X_1 \approx \frac{\varepsilon_{d\sigma} + \varepsilon_p}{2} + \sqrt{\left(\frac{\varepsilon_{d\sigma} - \varepsilon_p}{2}\right)^2 + 4V^2_{pd\sigma}}, \quad \text{(A30)}$$

where $\varepsilon_{d\sigma} = \varepsilon_d + 2V^2_{sd\sigma}/\Delta_{sd}$. From these equations, the parameters $V_{pd\sigma}$ and $V_{sd\sigma}$ can be obtained. Besides, there is also an additional equation for Γ_1

$$\Gamma_1 = \varepsilon_s. \quad \text{(A31)}$$

Substituting $\Delta_{sd} \equiv \varepsilon_d - \varepsilon_s \gg V_{sd\sigma}$ in Eq. (A29), we obtain

$$\Gamma_{12} = \frac{\varepsilon_d + \varepsilon_s}{2} + \left(\frac{\Delta_{sd}}{2}\right)\sqrt{1 + \frac{24V^2_{sd\sigma}}{\Delta^2_{sd}}} \approx \frac{\varepsilon_d + \varepsilon_s}{2} + \left(\frac{\Delta_{sd}}{2}\right)\left[1 + \frac{12V^2_{sd\sigma}}{\Delta^2_{sd}}\right] = \varepsilon_d + 6\frac{V^2_{sd\sigma}}{\Delta_{sd}}.$$

Hence,

$$E_{d_{eg}} \equiv \Gamma_{12} \approx \varepsilon_d + \frac{6V_{sd\sigma}^2}{\Delta_{sd}}. \tag{A32}$$

For the main text, we need an expression for Δ_σ

$$\begin{aligned}\Delta_\sigma &= (\Gamma_{12} - \Gamma_{25})/2 = (\Gamma_{12} - \varepsilon_p)/2 \\ &\approx \frac{1}{2}\left(\varepsilon_d + \frac{6V_{sd\sigma}^2}{\Delta_{sd}} - \varepsilon_p\right) \\ &= \Delta_\pi + 3V_{sd\sigma}^2/\Delta_{sd}.\end{aligned} \tag{A33}$$

Finally the hopping parameters of both models are given in Table III.

Remark. In the WE model, we use E_m as model parameter, hence $\Gamma \approx \varepsilon$, and in the Harrison model, we use ε_m as model parameter, hence $\Gamma = \varepsilon$. However. there is some contribution of the CF acting on the, e.g., p states at the Γ point: the interactions with Sr states, core states, Madelung potentials, etc. Therefore, ε_p is rather a model parameter than the true atomic energy, E_p, of a $2p$ state. If we speak about the model only, we may drop E_p and E_{t2g}, and retain only ε_p, ε_d, and E_{eg}.

TABLE III. Parameters of WE and Harrison models.

a	$V_{sd\sigma}$	$V_{pd\sigma}$	V_σ	$V_{pd\pi} = V_\pi$
3.9	2.9855	2.7237	2.0754	1.5590
4.0	2.7054	2.4064	1.8486	1.3854

[1] M. E. Lines and A. M. Glass, *Principles and Applications of Ferroelectrics and Related Materials* (Clarendon, Oxford, 1977).

[2] L. F. Mattheiss, E. M. Gyorgy, and D. W. Johnson, Phys. Rev. B **37**, 3745 (1988).

[3] Y. Moritomo, A. Asamitsu, H. Kuwahara, and Y. Tokura, Nature (London) **380**, 141 (1996).

[4] S. Ishihara, T. Hatakeyama, and S. Maekawa, Phys. Rev. B **65**, 064442 (2002).

[5] R. Cohen, Nature (London) **358**, 136 (1992).

[6] Y. A. Abramov, V. G. Tsirelson, V. E. Zavodnik, S. A. Ivanov, and I. D. Brown, Acta Crystallogr., Sect. B: Struct. Sci. **51**, 942 (1995).

[7] N. Sai and D. Vanderbilt, Phys. Rev. B **62**, 13942 (2000).

[8] R. Blinc, V. V. Laguta, B. Zalar, M. Itoh, and H. Krakauer, J. Phys.: Condens. Matter **20**, 085204 (2008).

[9] K. Koepernik and H. Eschrig, Phys. Rev. B **59**, 1743 (1999); http://www.FPLO.de

[10] J. P. Perdew and Y. Wang, Phys. Rev. B **45**, 13244 (1992).

[11] We also calculated the EFG for the low-symmetry phases of BTO and STO. Whereas the calculational results for BTO agree well with the experiment, the discrepancy for STO remains unchanged and of unclear reason.

[12] P. Blaha, K. Schwarz, and P. H. Dederichs, Phys. Rev. B **37**, 2792 (1988).

[13] L. F. Mattheiss, Phys. Rev. **181**, 987 (1969).

[14] L. F. Mattheiss, Phys. Rev. B **6**, 4718 (1972).

[15] L. F. Mattheiss, Phys. Rev. B **2**, 3918 (1970).

[16] T. Wolfram, Phys. Rev. Lett. **29**, 1383 (1972).

[17] T. Wolfram, E. A. Kraut, and F. J. Morin, Phys. Rev. B **7**, 1677 (1973).

[18] T. Wolfram and S. Ellialtioglu, Phys. Rev. B **25**, 2697 (1982).

[19] S. A. Prosandeev, A. V. Fisenko, and N. M. Nebogatikov, Sov. Phys. Solid State **29**, 2600 (1987).

[20] The parameters V_π and V_σ are from the WE (p-d) model and $V_{pd\pi} = V_\pi$ and $V_{pd\sigma}$ are from the Harrison (s-p-d) model, see Appendix, Sec. 3.

[21] W. A. Harrison, *Electronic Structure and the Properties of Solids* (Freeman, San Francisco, 1980).

[22] εdenotes the energy of the atomic level and E, as used before, denotes the energy-level corrected by the crystal field: $\Delta_\sigma = E_d - E_p = \varepsilon_d - \varepsilon_p + \delta_{\mathrm{CF},\sigma}$, cf. Eq. (A26). Note, that $\delta_{\mathrm{CF},m}$ is different for $m = \pi$ and $m = \sigma$, since ε_d is the atomic energy level and thus does not depend on m. This is the main reason, that, $\delta_{\mathrm{CF},\sigma} > \delta_{\mathrm{CF},\pi}$. Furthermore, $\delta_{\mathrm{CF},\sigma}$ has strong dependence on a.

[23] M. D. Kuzmin, A. I. Popov and A. K. Zvezdin, Phys. Status Solidi B **168**, 201 (1991).

[24] J. C. Slater, Phys. Rev. **78**, 748 (1950).

[25] The origin of the discrepancy with respect to the sign might be due to a different definition of the EFG in the applied codes.

[26] Note, that we use another sign in the definition of n^{Ew} compared to Ref 9 Eqs. (A30) and (A31).

[27] K. Koch, Ph.D. thesis, TU Dresden, 2009.